Calibration of optical tweezers with positional detection in the back focal plane

Simon F. Tolić-Nørrelykke, Erik Schäffer, Jonathon Howard, Francesco S. Pavone, Frank Jülicher, and Henrik Flyvbjerg

Citation: Review of Scientific Instruments **77**, 103101 (2006); doi: 10.1063/1.2356852

View online: https://doi.org/10.1063/1.2356852

View Table of Contents: http://aip.scitation.org/toc/rsi/77/10

Published by the American Institute of Physics

Calibration of optical tweezers with positional detection in the back focal plane

Simon F. Tolić-Nørrelykke[a),b)]
Max Planck Institute for the Physics of Complex Systems, Nöthnitzer Strasse 38, 01187 Dresden, Germany and European Laboratory for Non-linear Spectroscopy, via Nello Carrara 1, 50019 Sesto Fiorentino, Florence, Italy

Erik Schäffer[b)] and Jonathon Howard
Max Planck Institute of Molecular Cell Biology and Genetics, Pfotenhauerstrasse 108, 01307 Dresden, Germany

Francesco S. Pavone
European Laboratory for Non-linear Spectroscopy, via Nello Carrara 1, 50019 Sesto Fiorentino, Florence, Italy

Frank Jülicher
Max Planck Institute for the Physics of Complex Systems, Nöthnitzer Strasse 38, 01187 Dresden, Germany

Henrik Flyvbjerg
Isaac Newton Institute for Mathematical Sciences, Cambridge CB3 0EH United Kingdom; Biosystems Department, Risø National Laboratory, DK-4000 Roskilde, Denmark; and Danish Polymer Centre, Risø National Laboratory, DK-4000 Roskilde, Denmark

(Received 13 February 2006; accepted 26 August 2006; published online 9 October 2006; publisher error corrected 25 October 2006)

We explain and demonstrate a new method of force and position calibrations for optical tweezers with back-focal-plane photodetection. The method combines power spectral measurements of thermal motion and the response to a sinusoidal motion of a translation stage. It consequently does not use the drag coefficient of the trapped object as an input. Thus, neither the viscosity, nor the size of the trapped object, nor its distance to nearby surfaces needs to be known. The method requires only a low level of instrumentation and can be applied *in situ* in all spatial dimensions. It is both accurate and precise: true values are returned, with small error bars. We tested this experimentally, near and far from surfaces in the lateral directions. Both position and force calibrations were accurate to within 3%. To calibrate, we moved the sample with a piezoelectric translation stage, but the laser beam could be moved instead, e.g., by acousto-optic deflectors. Near surfaces, this precision requires an improved formula for the hydrodynamical interaction between an infinite plane and a microsphere in *nonconstant* motion parallel to it. We give such a formula. © *2006 American Institute of Physics.* [DOI: 10.1063/1.2356852]

I. INTRODUCTION

In order to use optical tweezers as a quantitative instrument for position and force measurements, the detection system must be calibrated. One calibration method interprets the power spectrum of thermal Brownian motion of a trapped object.[1–4] Another calibration method interprets the displacement of a trapped object in response to a known flow past it.[4–6] Both these methods require that the drag coefficient of the trapped object is known. Here we combine the two methods into one. Then there is no need to know the drag coefficient.

Mathematically speaking, the combined method measures an extra quantity that allows the elimination of the drag coefficient from the calibration procedure. This has some advantage: Methods that use the drag coefficient as input use the Stokes law to calculate it, hence rely on assumptions about the object's shape and radius and about the viscosity of the surrounding fluid. This contributes to the error on the final calibration, as do hydrodynamical interactions with nearby surfaces.[7]

With the combined method presented here, these sources of error have been eliminated. The drag coefficient of the trapped object can, in fact, be measured with the present method, and this with precision, as shown below. Finally, the method presented here is simpler to implement and requires less instrumentation than other methods that use additional lasers[8,9] or acousto-optic deflectors (AODs).[10]

II. MATERIALS AND METHODS

Measurements were done with two different optical tweezers systems. Both use the trapping laser for position detection in the back focal plane. One system has a long

[a)]Author to whom correspondence should be addressed; electronic mail: simonftn@pks.mpg.de
[b)]These authors contributed equally to this work.

working distance and was used to test the method far from surfaces (30 μm): This experimental setup is described in detail in Ref. 11 and briefly here. The instrument is based on a custom-built inverted microscope with a Nikon, 60×, 1.2 numerical aperture (NA), 0.2 mm working distance, Plan-Apo, water-immersion objective. The laser is a 1064 nm, Nd:YAG (Spectra-Physics Millennia IR). Position detection is done with a position-sensitive photodiode (UDT DLS-20). Flow cells with a volume of 10 μl (dimensions of $8\times20\times0.06$ mm^3) were assembled by placing a coverslip on top of a microscope slide separated by spacers of double-sided sticky tape. A dilute aqueous solution of beads was flowed in, and the ends were sealed with nail polish to avoid sample evaporation. The flow cell was mounted upside down on a Physik Instrumente piezoelectric translation stage (P-527.2 C1).

The other system has a short working distance and was used to test the method close to surfaces (0–3 μm): This experimental setup is described in detail in Ref. 12. Briefly, it consists of a modified Zeiss Axiovert 135 TV microscope equipped with a Zeiss, 100×, 1.3 NA, Plan-Neofluar, oil-immersion objective. The laser is a 1064 nm, Nd:YVO_4 (Smart Laser Systems GmbH, Berlin, Germany). Position detection is obtained with a standard quadrant photodiode, QP50-6SD (Pacific Silicon Sensors Inc.). Signals were recorded with a 24 bit data acquisition card (NI 4472, National Instruments) which has a 45 kHz alias-free bandwidth. Temperature was measured with type-*T* thermocouples, accurate to within 0.1 °C (IT-23 Physitemp, Clifton, NJ, U.S.A.). Flow cells with a 3-mm-wide channel were assembled by placing a 18 mm^2 coverslip on top of a No. 1.5 22 mm^2 coverslip separated by a layer of Parafilm. The Parafilm was melted by placing the sample on a 100 °C hot plate. Cooling then glued the coverslips together. Microspheres suspended in an aqueous 0.1 M KCl solution were flowed in, and the ends were sealed with vacuum grease to avoid sample evaporation. The flow cell was mounted on a Physik Instrumente piezoelectric translation stage (P-733.2 CL) with built-in capacitance position detection precalibrated to within 0.1%. For measurements close to the surface, the coverslips were coated with Pluronic® F127 (Sigma) on top of a thin polymer layer (Teflon® AF 1600, DuPont) as described in Ref. 12. This protocol minimized static bead-surface interactions.

The following beads were used: silica beads from Bangs Laboratories (Fishers, IN, USA), catalog code SS04N, lot number 5303, were 1.54 μm in diameter with a coefficient of variation (standard deviation divided by the mean value) of 10% listed by the manufacturer. Polystyrene microspheres from Polysciences (Warrington, PA, USA), catalogue number 07307, lot number 50602, were 528 nm in diameter with a 2% coefficient of variation listed by the manufacturer. Transmission electron microscopy (TEM) of the latter microspheres indicated a 1.2% coefficient of variation.

III. THEORY

In the following we present the theory for a calibration procedure in which the flow cell is moved sinusoidally a known distance relative to the trapping laser by a piezoelectric translation stage. If, instead, the trap is moved a known distance relative to the flow cell, the same formulas apply, provided that the detector is placed in the back focal plane of the condenser.

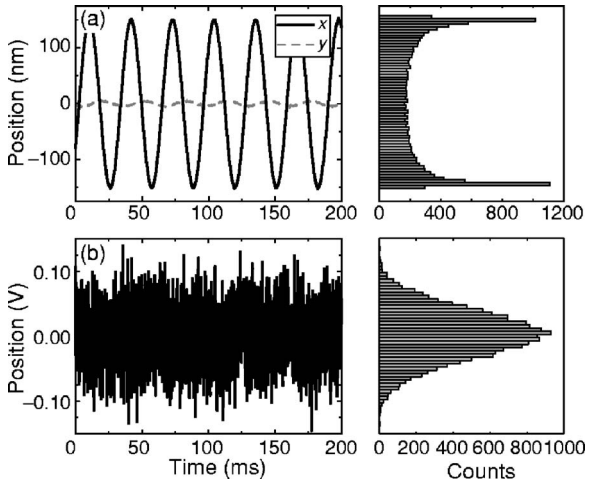

FIG. 1. Positions of the piezostage (a) and the trapped bead (b) for a stage moving sinusoidally with frequency $f_{\mathrm{drive}}=32$ Hz and amplitude $A=150$ nm in the x direction. (a) Left, time series of stage position; right, histogram of the x coordinate of the stage position. The sinusoidal movement results in two clear maxima. (b) Left, time series of the bead's x coordinate in volts, as given by the signal from the photodiode. The amplitude of the sinusoidal response is smaller than the amplitude of the thermal motion. Consequently the sinusoidal shape is masked by the Brownian motion of the bead, and the maxima associated with the sinusoid disappear in the histogram of visited positions (right).

In order to keep the presentation as simple as possible, we use Einstein's simple theory for Brownian motion. The presentation given here carries over unchanged to the full, hydrodynamically correct theory, including possible filters, electronic and/or parasitic.[2,3] We present the relevant formulas in Appendix D.

A. Equation of motion

A microsphere suspended in water is trapped with optical tweezers inside a flow cell. The stage moves the flow cell sinusoidally relative to the optical trap with a frequency f_{drive} and an amplitude A, see Fig. 1, while the trap remains at rest in the laboratory system. The position of the stage as a function of time t is

$$x_{\mathrm{drive}}(t) = A\,\sin(2\pi f_{\mathrm{drive}} t). \tag{1}$$

The stage velocity $v_{\mathrm{drive}}(t) \equiv \dot{x}_{\mathrm{drive}}(t)$ also corresponds to the velocity of the water in the flow cell far away from the bead, since the water is at rest relative to the flow cell (see Appendix B). Ignoring hydrodynamical and inertial effects, the Langevin equation of motion for a spherical bead in the trap is

$$\gamma[\dot{x}(t) - v_{\mathrm{drive}}(t)] + \kappa x(t) = F_T(t), \tag{2}$$

where $x(t)$ is the position of the bead relative to the center of the trap, γ is the drag coefficient, and κ is the trap stiffness. The first term on the left-hand side is the drag force, which is proportional to the velocity of the bead relative to that of the stage. The second term on the left-hand side is the trapping force. The right-hand side is the random thermal force driv-

ing the Brownian motion. It is assumed to have the statistical properties of white noise,

$$F_T(t) = \sqrt{2\gamma k_B T}\xi(t) = \gamma\sqrt{2D}\xi(t), \tag{3}$$

where $k_B T$ is the Boltzmann energy at absolute temperature T, the diffusion coefficient is given by Einstein's relation $D = k_B T/\gamma$, and ξ is the normalized white noise expressed with Dirac's delta function δ,

$$\langle \xi(t) \rangle = 0, \quad \langle \xi(t)\xi(t') \rangle = \delta(t - t'). \tag{4}$$

Here $\langle \cdots \rangle$ denotes the expectation value that results from averaging over the thermal noise.

B. Solution to the equation of motion

Since the equation of motion (2) is linear with two force terms, F_T and γv_{drive}, its general solution can be written as a sum of two terms, one for each force,

$$x(t) = x_T(t) + x_{\text{response}}(t), \tag{5}$$

after transient initial behavior has died out. Here,

$$x_T(t) = \sqrt{2D}\int_{-\infty}^{t} dt' e^{-2\pi f_c(t-t')}\xi(t'), \tag{6}$$

$$x_{\text{response}}(t) = \frac{x_{\text{drive}}(t - t_{\text{lag}})}{\sqrt{1 + (f_c/f_{\text{drive}})^2}}, \tag{7}$$

where we have introduced the corner frequency $f_c = \kappa/(2\pi\gamma)$ and $t_{\text{lag}} = [\arctan(f_{\text{drive}}/f_c) - \pi/2]/(2\pi f_{\text{drive}})$. Figure 1(b) shows an example of an experimentally determined trajectory $x(t)$ of a bead in a trap, as described in Eq. (5). In this case, the stochastic thermal motion dominates and almost hides the driven, deterministic component of the motion.

In principle, we now could calibrate by fitting $x_{\text{response}}(t)$ in Eq. (7) to data like those shown in Fig. 1(b). However, this is not a reliable procedure.[13] Instead, we Fourier transform theory and data to the frequency domain where parameters are determined with optimal precision because the theory is simpler there.

C. Power spectrum

From Eqs. (5) and (6) it follows that the Fourier transform of $x(t)$ is

$$\hat{x}(f) = \int_{-\infty}^{\infty} dt\ e^{i2\pi ft}x(t) = \frac{\hat{\xi}(f)\sqrt{2D}}{2\pi(f_c - if)} + \frac{Ae^{i2\pi f t_{\text{lag}}}}{2i\sqrt{1 + (f_c/f_{\text{drive}})^2}}[\delta(f + f_{\text{drive}}) - \delta(f - f_{\text{drive}})], \tag{8}$$

where $\hat{\xi}(f)$ is the Fourier transform of $\xi(t)$. Consequently, the expectation value for the one-sided ($f \geqslant 0$) power spectral density (PSD) of the bead positions is[14]

$$P(f) = \frac{2\langle|\hat{x}(f)|^2\rangle}{t_{\text{msr}}} = P_T(f) + P_{\text{response}}(f) \xrightarrow[t_{\text{msr}}\to\infty]{} \frac{D}{\pi^2(f^2 + f_c^2)} + \frac{A^2}{2(1 + f_c^2/f_{\text{drive}}^2)}\delta(f - f_{\text{drive}}), \tag{9}$$

where t_{msr} is the measurement time [see also Eq. (8) of Ref. 2]. This PSD consists of the familiar Lorentzian (first term, P_T), *plus* a delta-function spike (second term, P_{response}) at the frequency with which the stage is driven. The Lorentzian originates from the Brownian motion of the bead in the parabolic trapping potential and is hereafter referred to as the "thermal background."

IV. HOW TO CALIBRATE

Experimentally, positions are measured in volts, x^{volt}. Assuming linearity,[11,12]

$$x(t) = \beta x^{\text{volt}}(t), \tag{10}$$

positions are known in meters once the calibration factor β has been determined. It can be determined from the measured PSD: From Eq. (10) it follows that the experimental PSD P^{volt} is measured in $\text{V}^2\,\text{s}$ and

$$P_{\text{response}}(f) = \beta^2 P^{\text{volt}}_{\text{response}}(f). \tag{11}$$

Here, $P^{\text{volt}}_{\text{response}}$ is known experimentally and, as can be seen from Eq. (9), so is P_{response}, since A and f_{drive} are known *a priori* and f_c is known experimentally. So the calibration factor β is the only unknown in Eq. (11), hence determined by this equation.

In practice the experimental measurement time is always finite. This is taken into account in the expression for β given below.

The procedure described here works in bulk and near a surface. If used near a surface, the resulting calibration is specific to the distance from the surface, so is the value found for the drag coefficient. Faxén's law [Eq. (D5) below] and formulas in Ref. 12 and in Sec. 7.4 of Ref. 15 relate the drag coefficient to its bulk value for the lateral and axial directions, respectively.

A. Positional calibration

The desired calibration factor for distances is

$$\beta = \sqrt{W_{\text{th}}/W_{\text{ex}}}, \quad [\beta] = \text{m/V}, \tag{12}$$

where W_{ex} is the experimentally determined power in the spike, measured in V^2, and W_{th} is the same quantity measured in m^2. The latter follows from Eq. (9),

$$W_{\text{th}} = \int_0^{f_{\text{Nyq}}} P_{\text{response}}(f)df = \frac{A^2}{2(1 + f_c^2/f_{\text{drive}}^2)}, \tag{13}$$

whereas W_{ex} is found by observing that in an experiment the measurement time t_{msr} is not infinite, so the spike is no longer a delta function. As detailed in Appendix C, its height is now proportional to t_{msr}, and its width is also finite in general. However, if t_{msr} is an *integer multiple* of the period

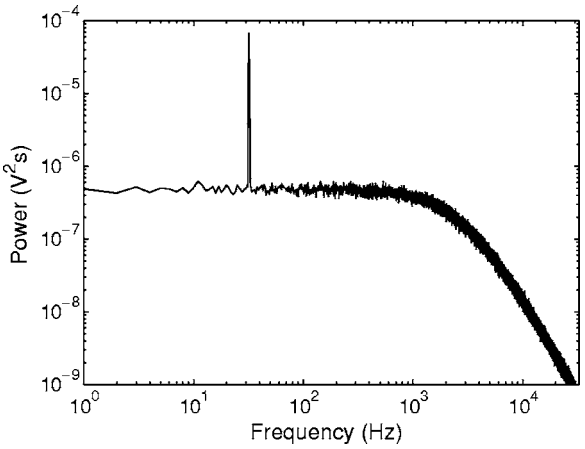

FIG. 2. Power spectrum of a 528 nm diameter polystyrene bead held in the laser trap with a corner frequency $f_c=2065\pm5$ Hz. The sample moves sinusoidally with amplitude $A=150$ nm and frequency $f_{\text{drive}}=32$ Hz. The power spectrum shown is the average of 100 independent power spectra. It consists of a thermal background caused by Brownian motion, plus a spike at f_{drive}. The sampling frequency was $f_{\text{sample}}=65\,536$ Hz, the measurement time for each spectrum was $t_{\text{msr}}=1$ s, and the temperature was 24.4 °C. For a clear illustration, the measurement time used here is eight times longer than the one we typically use for calibration.

of the stage movement, then the spike consists of a single datum,[16] see Fig. 2, and consequently

$$W_{\text{ex}}=[P^{\text{volt}}(f_{\text{drive}})-P_T^{\text{volt}}(f_{\text{drive}})]\Delta f, \tag{14}$$

where $P^{\text{volt}}(f_{\text{drive}})$ is the height of the spike, i.e., the experimentally determined value of the PSD at f_{drive}, and $P_T^{\text{volt}}(f_{\text{drive}})$ is the PSD of the thermal background at f_{drive}. Both are measured in V^2 s. The width $\Delta f=1/t_{\text{msr}}$ corresponds to the frequency resolution of the PSD.

The thermal background in this expression can be treated with three different levels of precision: (i) Do not subtract it at all, if it is truly negligible compared to the height of the spike. (ii) Interpolate its value from a plot of the power spectrum. This approach can also be taken if the PSD is contaminated with low-frequency power, that is external to the model used here, e.g., from electronic noise or the pointing instability of the laser beam. (iii) Use the value at f_{drive} of the theoretical expression for the thermal background $P_T^{\text{volt}}(f)$ after it has been fitted to the experimental thermal background.

B. Force calibration

The trap's force on a bead is κx. With the position detection system calibrated, the displacement x is measured in meters. To determine the trap stiffness κ, we use the definition of f_c and Einstein's relation to write $\kappa=2\pi f_c k_{\text{B}}T/D$. Next, we determine f_c and D^{volt}, the diffusion constant in V^2/s, by fitting the first term in Eq. (9) to the thermal background in the experimental PSD. Using $D=\beta^2 D^{\text{volt}}$, we arrive at a practical formula for force calibration:

$$\kappa_{\text{ex}}=2\pi f_c\frac{k_{\text{B}}T}{\beta^2 D^{\text{volt}}}. \tag{15}$$

All variables on the right-hand side are measured experimentally in the calibration process. The local temperature T of the liquid can typically be determined with sufficient accuracy by direct measurement in or near the flow cell: T is the absolute temperature, so an absolute error of 1 K results in a relative error of only 0.3%.

As a side effect of this calibration procedure, we find an experimental result for the drag coefficient,

$$\gamma_{\text{ex}}=\frac{k_{\text{B}}T}{\beta^2 D^{\text{volt}}}, \tag{16}$$

where again all variables on the right-hand side are measured experimentally in the calibration process.

Use of the hydrodynamically correct theory for Brownian motion changes Eq. (12) only by replacing W_{th} with $W_{\text{th,hydro}}$ (see Appendix D). The values found for κ_{ex} and γ_{ex} with these equations do change, because more correct values for f_c and D^{volt} result from fitting the thermal background with the hydrodynamically correct theory. The value found for W_{ex} is also affected a little through the subtraction of the thermal background in Eq. (14).

V. EXPERIMENTAL RESULTS

In order to test the accuracy and advantage of the calibration method described above, we here compare our experimentally determined values for the drag coefficient with values calculated from vendor information. Deep in bulk, 21 silica beads with a diameter of 1.54 μm were studied with an optical tweezers system with a water-immersion objective. At various distances close to the coverslip (<3 μm), 24 polystyrene beads with a diameter of 528 nm were studied with an optical tweezers system with an oil-immersion objective. Fitting of the PSD to the thermal background recorded for each bead at each of its positions considered was done with the highest possible precision, using either published MATLAB routines[17,18] or custom-written software in LABVIEW.[12] These fitting routines take into account hydrodynamic corrections, aliasing, parasitic filtering in the photodiode, and electronic filters in the data acquisition system.[2,3]

A. Measurements in bulk

First we measured the drag coefficient far from surfaces, where γ_{ex} can be compared directly to Stokes's formula $\gamma_0=6\pi\eta R$, with the bead diameter $2R=1.54$ μm taken from the specifications of the producer and the viscosity $\eta=0.93$ mPa s calculated for water at the measured temperature, 23.0 °C. Beads were trapped near the bottom of the flow chamber (silica beads are heavier than water) and brought to the middle of the flow cell, 30 μm from the bottom and the top, to minimize the effect of nearby surfaces. The x axis—the direction of motion—was chosen perpendicular to the long axis of the flow cell and perpendicular to the direction of the incoming laser light (the z axis). The experimental parameters were $A=208$ nm and $f_{\text{drive}}=28$ Hz. For each of the 21 beads, f_c, D^{volt}, and W_{ex} were determined from its power spectrum recorded in bulk.

The average of values measured for γ_{ex} was $\overline{\gamma_{\text{ex}}}=13.4\pm0.2$ nN s/m [mean±standard error (SE) on the mean, $n=21$ beads], and the standard deviation (SD) of measured values for γ_{ex} was 0.8 nN s/m, i.e., the measured drag coefficient showed a coefficient of variation of 6%, which is consistent with the 10% variation in bead diameter listed by

the manufacturer because of our limited sample size. The value for the average drag coefficient expected from the manufacturer's information is 13.5±0.3 nN s/m (mean±SE), where the SE was obtained by adding the errors associated with viscosity and variation in bead diameter in quadrature divided by n. These results suggest that our calibration method is both accurate and precise.

B. Measurements near surfaces

In practice, experiments are often done close to a surface, such as a coverslip. Working close to a surface—in our case <3 μm—complicates standard calibration techniques, especially if a high numerical aperture oil-immersion objective is used. In that case aberrations arising from a refractive index mismatch at the glass-water interface cause a linear decrease in stiffness away from the surface and a focal shift.[19–21]

1. Acquisition and fitting

The experimental parameters were $A=150$ nm, $f_{\text{drive}}=32$ Hz, $f_{\text{sample}}=65\,536$ Hz, $t_{\text{msr}}=1/8$ s, and $T=24.4$ °C. The beads used had, according to the producer, a diameter of $2R=528$ nm with a 2% coefficient of variation. Power spectra that resulted from averaging 100 independent spectra were fitted with a custom-written least-squares fitting routine implementing a Levenberg-Marquardt algorithm (LABVIEW, NI). Each datum was weighted by its theoretical error bar.[2] The propagated error on the fit parameters was calculated as the square root of the diagonal elements of the covariance matrix multiplied by the reduced χ^2 value. The fit was done in the frequency interval [8 Hz:25 kHz], omitting the single datum at the stage frequency $f_{\text{drive}}=32$ Hz and using Eq. (D2) for the thermal background, with Eq. (35) in Ref. 2 describing parasitic filtering.

For every trapped bead the calibration factor β, the trap stiffness κ_{ex} and the drag coefficient γ_{ex} were found at each of 50 distances from the surface. The exact surface position was obtained from a fit of Faxén's law to the measured drag coefficients, taking the focal shift into account; see Appendix D and Ref. 12. Thus, the quoted values for γ_{ex} are the measured values extrapolated to bulk, hence directly comparable to γ_0.

2. Temperature

We measured the temperature with a small thermocouple introduced into the flow cell, while simultaneously recording the room temperature and the temperature of the imaging and condenser objectives. The temperatures of these two objectives differed by 0.5 °C. The temperature inside the flow cell was intermediate between these and was measured to within 0.2 °C. We estimated an upper limit of 0.5 °C for the local temperature increase due to laser heating.[22] Thus, the propagated error on γ_{ex} in Eq. (16) would be less than 0.2% if the uncertainty about the temperature were the only source of error.

3. Drag coefficient

Figure 3 shows the experimentally determined values for the drag coefficient γ_{ex}, here given in units of the theoretically expected drag coefficient, γ_0, for 24 individual beads. The error bars on the individual data points are the propagated errors from the fit to Faxén's law and the uncertainty in the temperature. This high precision results from the long measurement time and the 50 determinations of γ_{ex} for each bead. Any systematic error—e.g., an undetected error in the specifications of the piezostage—will offset the mean value of γ_{ex}, but will not change the position of the data points relative to each other. In other words, systematic errors directly influence the accuracy of the method, but do not influence the precision. We check the accuracy by comparing γ_{ex} to γ_0, including its estimated errors. The shaded area shows the 2.3% error on γ_0 from the propagated uncertainty on the viscosity (temperature) and the bead radius.

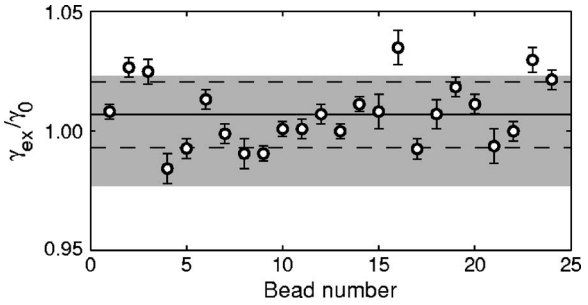

FIG. 3. Results from the calibration of 24 individual beads trapped close to a surface. The circles show the measured drag coefficients Eq. (16), extrapolated to their bulk values according to Faxén's law, in units of the theoretically expected drag coefficient in bulk. The error bars are the propagated errors from the fitting routines used. The horizontal solid line and the two dashed lines denote the mean $(\overline{\gamma_{\text{ex}}})$±SD of the 24 measurements. The accuracy of the method is illustrated by the agreement of the two values $\overline{\gamma_{\text{ex}}}/\gamma_0=1.007\pm0.003$ (mean±SE). The shaded region denotes the estimated 2.3% uncertainty on γ_0.

The average of the measured values for the 24 beads, $\overline{\gamma_{\text{ex}}}$, was 1.007±0.003 (mean±SE, $n=24$) in units of γ_0. As seen in Fig. 3, the experimental value for an individual bead may differ several percent from the theoretically expected value γ_0, even if the average value does not. Thus, if γ_0 is used for calibration, stochastic errors of several percent are expected due to the polydispersity of the bead radii.

We were able to measure the polydispersity of the bead population because the precision of our calibration method (error bar on single-bead datum) was smaller than this polydispersity. The coefficient of variation of the bead population's various γ_{ex} values was 1.5%, which is comparable to the 2% coefficient of variation for the bead diameter listed by the producer and the 1.2% measured independently by us using TEM.

VI. DISCUSSION

The main strength of the calibration method presented here is that it is independent of estimates regarding the drag coefficient and that it can be performed on the location of the experiment. It shares this strength with other methods,[9,10] but unlike those it does not require two laser beams or AODs.

The method presented here has some resemblance to a method used in Refs. 23 and 24. There, a bead embedded in a gel was driven sinusoidally through the detection laser, and

the resulting spike in the PSD was used to estimate the sensitivity of the detection system. However, that method was not *in situ* since the bead used for the calibration could not be used for later experiments.

In Appendix A we discuss a number of issues associated with the use of optical tweezers, in general, and our implementation of the calibration method, in particular.

VII. CONCLUSION: RECOMMENDED APPROACH

We suggest the following steps in experiments using a piezoelectric translation stage.

(1) Trap the object of interest at the position of interest.
(2) Drive the stage at any frequency f_{drive} that does not excite resonances in the system. We typically used 16 or 32 Hz, low enough that the fluid moves with the stage (see Appendix B).
(3) Collect position data from the photodetection system and the piezostage for a time t_{msr} that is an integer number of stage periods—i.e., $t_{\mathrm{msr}}f_{\mathrm{drive}}=$integer—to avoid leakage and with a sampling frequency that makes the number of data points, $t_{\mathrm{msr}}f_{\mathrm{sample}}$, a power of 2, so the PSDs of positions can be obtained by fast Fourier transform (FFT).
(4) Determine A and f_{drive} from the PSD of the piezostage positions (or use previously calibrated values).
(5) Determine D^{volt} and f_{c} from a fit to the thermal background in the PSD of the bead positions.
(6) Determine the value of the spike in the PSD at f_{drive} and calculate β and κ using Eqs. (12) and (15).

In point 2, the suggested values for f_{drive} are powers of 2 for ease of calculation of the appropriate t_{msr} and f_{sample}. In point 5, we recommend using the full theory for fitting the PSD if less than 10% systematic error is desired. The relevant equations are given in Appendix D, in Refs. 2 and 3, and software in Refs. 17 and 18.

VIII. OUTLOOK

A. Calibration of the axial direction

The total intensity of the laser light that impinges on the position detector in the back focal plane contains information about the displacement of the trapped object in the axial direction, i.e., in the direction of the optical axis, the z axis.[25] It is generally possible to calibrate this dimension by moving the sample relative to the laser along the z axis. If AODs are used to move the laser relative to the trapped object,[10] this is impossible. However, for spherical objects the bulk drag coefficient is the same in all directions, and it is sufficient to determine the drag coefficient in one dimension in order to calibrate all three dimensions. When working close to a surface, the drag coefficient depends on the direction of motion. However, if the bead is spherical and the distance to the surface is known or determined as, e.g. in Sec. V B, it is again sufficient to determine the drag coefficient in just one direction. Faxén's law and formulas given in Ref. 12 and in Sec. 7.4 of Ref. 15 can be used to correct for the distance dependence of the drag coefficient for the remaining lateral and/or axial dimensions, respectively, depending on which dimension was previously calibrated. This latter procedure has been experimentally verified in Ref. 12. The precision and accuracy were the same as for the lateral directions.

B. Imaging versus nonimaging positional detection

Here we demonstrated our method using positional detection in the nonimaging back focal plane of the condenser. In the back focal plane an interference pattern is detected. This pattern arises as the laser light scattered from the bead interferes with the unscattered laser light.

Position detection in the image plane should also work, if the laser trap remains stationary in the laboratory coordinate system, while the flow cell is driven. For example, an image of the bead could be projected onto a photodiode or a camera. With such a setup, calibration can also be obtained by simply moving the detector a known distance relative to the image while recording the response.[26]

Another approach moves the trapping laser relative to the flow cell, e.g., using AODs, galvano mirrors, or some other beam-steering apparatus.[1,10] This approach works if back-focal-plane detection is used: A pure translation of the laser in the image plane produces no signal in the back focal plane, and only a motion of the trapped object relative to the laser is detected. An advantage of this approach is that open samples can be used because the sample is not moving.

C. *In situ* measurements

The method presented here is implemented strictly *in situ*. Therefore, it should be applicable in situations that have so far eluded accurate measurements of positions and forces, e.g., when trapping spherical structures of unknown refractive index and size in the interior of cells. The method described here could also be used in microfluidic lab-on-a-chip devices, for measuring forces, viscosities, or temperatures inside micron-sized channels. Generally, position and force calibrations should be possible in an arbitrary geometry, because we do not need to know the corrections to the drag coefficient due to the proximity of surfaces in the approximation used in Eq. (2), where the frequency dependence of the drag coefficient is neglected. More generally, all that is needed for the present method to apply with precision is a system that displays a linear response to forces, as in Eq. (2): The drag should be proportional to the trapped object's velocity, but may depend on frequency as in Appendix D as long as the functional form of the frequency dependence is known, or can be modeled, and the trapping force should be Hookean.

ACKNOWLEDGMENTS

The authors thank Kirstine Berg-Sørensen for critical reading of the article. Two of the authors (H.F. and F.J.) thank the *Isaac Newton Institute for Mathematical Sciences* and its program *Statistical Mechanics of Molecular and Cellular Biological Systems* for hospitality while this work was initiated. One of the authors (H.F.) thanks Steve Block for the opportunity to present an early version of the present work at his Winter Workshop on Biophysics, (Ref. 43). An-

other author (S.F.T.-N.) thanks Marco Capitanio for technical assistance.

APPENDIX A: EXPERIMENTAL ISSUES

We considered the following issues in the implementation of our calibration method.

(1) *Stage response.* Piezostages have a finite response time, but this is not a problem here, since we drive with a sinusoidal signal. This is the signal, which another periodic signal will degenerate towards, if its period is shorter than the response time of the stage. Also, any deviation from the chosen signal shows up in the experimental power spectrum as distinct, isolated higher modes at frequencies that are integer multiples of the driving frequency.
Mechanical resonances of the experimental setup can be excited. Our setups have resonance frequencies starting at approximately 400 Hz. The excitation of a resonance will give rise to additional power in the PSD at the resonance frequency, hence is under experimental control. Mechanical cross-talk between axes occurs, as seen in Fig. 1. However, as the equations of motion are linear, this does not influence the calibration.

(2) *Photodiode response*. Photodiodes may act as filters, but the effect is well understood and can be measured and accounted for.[2,3,27] Depending on the type of diode used (quadrant or position sensitive), the linearity of the response to bead displacements may also vary. The region of linearity is easily found by moving a stuck bead through the laser focus. The photodiode must be aligned with the piezostage. This is achieved by driving the stage along one of its axes while rotating the diode until the power at the driving frequency is maximized for the corresponding axis.

(3) *Cross-talk*. Cross-talk between the axial (z) and the lateral (x and y) channels from a quadrant photodiode may lead to underestimates of f_c of up to 10%. This cross-talk shows up as additional power in the PSD of the x, y channels. Since the axial corner frequency is smaller than the lateral ones,[28] cross-talk raises the plateau of the lateral signals. A likely source of the cross-talk is the differences in amplification of the signals from the diode's four quadrants. By repositioning the diode relative to the laser so that a small offset from the center position (i.e., zero volts in x and y) is introduced, the cross-talk can be minimized by maximizing the lateral corner frequencies that are returned from fits to the PSD.[2,12]

(4) *Laser heating of the liquid*. The laser heats up the liquid locally, resulting in a decrease in viscosity. We looked for this effect by varying the laser intensity, but did not find any such effect when working close to surfaces. This result is to be expected because the glass coverslip acts as a heat sink.[22]

(5) *Hydrodynamic response of the sample*. The calibration method presented here is conditioned on the liquid comoving with the stage. In Appendix B we calculate the response of the liquid to the oscillatory movement of the stage. Close to the surface, the no-slip boundary condition entrains the liquid. Further into the sample, the degree of entrainment depends on the height of the sample d and the drive frequency. If $d^2\pi f_{\mathrm{drive}} < \nu \approx 1\ \mathrm{mm}^2/\mathrm{s}$, where ν is the kinematic viscosity, the liquid comoves in the entire flow cell.

(6) *Shape of the trapped object*. The only demand on the trapped object is that it does not rotate in response to forced movement, at least not in a manner that gives rise to a response in the detection system. This condition is fulfilled if the particle is spherical, or asymmetric but strongly trapped. Due to the height dependence of the drag coefficient, even a spherical bead rotates when translated close to a surface. However, this rotation dissipates a negligible amount of energy compared to the translational dissipation[15] and hence does not affect the calibration. If the trapped object is elongated and weakly trapped, it may wobble in the trap in response to the oscillating liquid and give rise to detection of false movement by the photodiode. But this is not a problem with commercial microspheres because they are highly spherical, as are many small biological objects such as lipid droplets or vesicles.

(7) *Shape of the trapping potential*. Throughout this article we assumed a parabolic trapping potential, but the method is not limited by this assumption. By choosing large drive amplitudes A, it is possible to map the shape of the potential and calibrate it. This is done by analyzing the higher modes of the bead's motion that arise in response to a sinusoidal drive in a nonlinear trapping force field.

APPENDIX B: HYDRODYNAMICS

Sometimes it is desirable to work with a flow cell with *open ends*, e.g., to facilitate the exchange of buffer solutions. When the ends are open, the liquid between the two coverslips generally does not move with the same amplitude or phase as the flow cell.

To estimate the size of this effect, we consider the motion of a liquid contained between two infinite, parallel planes which are moved identically, parallel to themselves, in a simple sinusoidal fashion. In an experiment, two of the four sides of the flow cell are sealed, which increases the drag force on the liquid. Also, the surface tension at the openings helps force the liquid to move with the flow cell. Thus, the result below for two infinite, parallel planes exaggerates the liquid's motion—it is a worst-case scenario.

The velocity of the oscillating planes (the coverslips) is zero in the y and z directions, and

$$v_{\mathrm{drive}} = \omega A \cos(\omega t) \tag{B1}$$

in the x direction, where $\omega = 2\pi f_{\mathrm{drive}}$. The only external forces on the liquid are the shear forces arising from the no-slip boundary condition between the liquid and the accelerated planes. The liquid moves with the accelerated planes with a time lag determined by the balance between the inertia of the liquid and the shear forces inside the liquid. Thus, we see that the velocity of the liquid can be written as $\mathbf{u}(x,y,z,t) = (u(z,t),0,0)$.

The equation of motion for the liquid is obtained from the linearized Navier-Stokes equations with constant pressure (see Ref. 29):

$$\frac{\partial u}{\partial t}(z,t) = \nu \frac{\partial^2 u}{\partial z^2}(z,t), \tag{B2}$$

where ν is the kinematic viscosity of the liquid. The relevant solution to this equation can be written as

$$u(z,t) = a(z)\cos(\omega t) + b(z)\sin(\omega t) \tag{B3}$$

$$= A_{\text{liquid}}(z)\cos(\omega(t - t_{\text{phase}}(z))), \tag{B4}$$

where $A_{\text{liquid}} = \sqrt{a^2 + b^2}$ and $\omega t_{\text{phase}} = \arctan(b/a)$. The coefficients a and b can be found by substituting Eq. (B3) into Eq. (B2):

$$a = -\frac{\nu}{\omega} b'' \quad \text{and} \quad b = \frac{\nu}{\omega} a'', \tag{B5}$$

from which we find

$$a'''' = -\left(\frac{\omega}{\nu}\right)^2 a, \tag{B6}$$

where the prime ($'$) indicates differentiation with respect to z. The solution to Eq. (B6) is a linear combination of $\exp\{[(\pm 1 \pm i)/\sqrt{2}]\sqrt{\omega/\nu} z\}$ whose four coefficients are determined by the symmetry requirement $a(z) = a(d - z)$ and the boundary conditions $a(0) = \omega A$ and $a''(0) = 0$:

$$a(z) = c_1 \cos\left(\frac{z - d/2}{\zeta}\right)\cosh\left(\frac{z - d/2}{\zeta}\right) + c_2 \sin\left(\frac{z - d/2}{\zeta}\right)\sinh\left(\frac{z - d/2}{\zeta}\right), \tag{B7}$$

where

$$c_1 = \omega A \frac{\cos(d/2\zeta)\cosh(d/2\zeta)}{\cos^2(d/2\zeta) + \sinh^2(d/2\zeta)}, \tag{B8}$$

$$c_2 = \omega A \frac{\sin(d/2\zeta)\sinh(d/2\zeta)}{\cos^2(d/2\zeta) + \sinh^2(d/2\zeta)}, \tag{B9}$$

and

$$\zeta = \sqrt{2\nu/\omega} \tag{B10}$$

is the depth of penetration of the shear wave into the fluid. The expression for b follows from Eq. (B5) and is identical to Eq. (B7) except for c_1 and c_2 swapping places. When $d \gg \zeta$ the shear wave's amplitude decreases exponentially as a function of z. When $d \ll \zeta$ the liquid comoves with the planes as a solid body.

With the parameters used in the experiment far from surfaces, described in Sec. V, i.e., $f_{\text{drive}} = 28$ Hz, the penetration depth $\zeta = 103$ μm is larger than the thickness of the flow cell $d \simeq 60$ μm. With these parameters, the amplitude of the liquid's motion differs at most 0.25% from the amplitude of the stage's motion (see Fig. 4). This result is independent of the amplitude A but is quite sensitive to d and f_{drive}. Thus, if working away from the surface it is important to choose f_{drive} so that it matches the thickness of the cell, i.e., so that $d/\zeta < 1$.

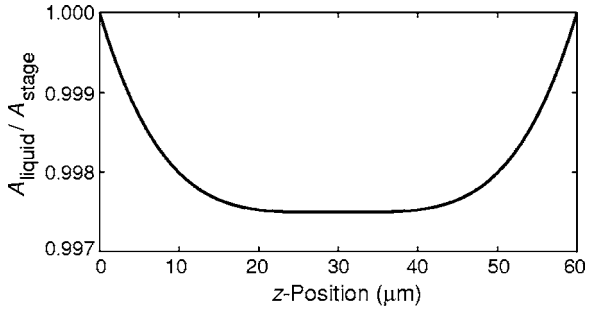

FIG. 4. Hydrodynamic prediction of the response of the liquid to the motion of the coverslips. Abscissa: Height above coverslip z. Ordinate: Amplitude of liquid motion $A_{\text{liquid}}(z)$, Eq. (B4), in units of the amplitude of the oscillating planes $A_{\text{stage}} = A$. Parameters are the same as used in the experiment far from surfaces ($f_{\text{drive}} = 28$ Hz, $A = 208$ nm, $T = 23.0$ °C).

It is illustrative to calculate the velocity of the liquid midway between the two planes, since this is where the motion of the liquid differs the most from that of the planes:

$$u\left(\frac{d}{2}, t\right) = c_1 \cos(\omega t) + c_2 \sin(\omega t) \tag{B11}$$

$$= A_{\text{liquid}}\left(\frac{d}{2}\right)\cos(\omega(t - t_{\text{phase}}(d/2))), \tag{B12}$$

where now $A_{\text{liquid}}(d/2) = \sqrt{c_1^2 + c_2^2}$ and $\omega t_{\text{phase}}(d/2) = \arctan(c_2/c_1)$. When the coverslips are close together or the drive frequency is very low $d/2\zeta \ll 1$, and we have $u(d/2, t) = v_{\text{drive}}(t)$, i.e., the fluid comoves with the planes. If the coverslips are far apart or the drive frequency is high Eq. (B12) becomes

$$u\left(\frac{d}{2}, t\right) = 2\omega A e^{-d/2\zeta}\cos(\omega t - d/2\zeta), \quad d \gg 2\zeta, \tag{B13}$$

i.e., the amplitude decreases exponentially as d/ζ grows and the motion of the liquid is phase shifted relative to the motion of the planes. These behaviors are illustrated in Fig. 5.

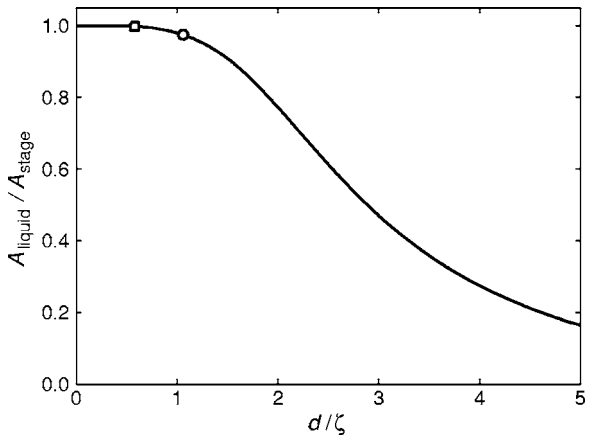

FIG. 5. Hydrodynamic prediction of the amplitude of liquid motion midway between the two coverslips. Abscissa: The distance between two planes d, measured in units of the penetration depth ζ, Eq. (B10). Ordinate: Amplitude of the liquid oscillations midway between the two planes $A_{\text{liquid}}(d/2)$, Eq. (B12), in units of the amplitude of the oscillating planes $A_{\text{stage}} = A$. Notice the plateau at unity for small values of d/ζ where the fluid moves with the planes and the exponential decay to zero at larger values where the liquid no longer follows the planes. The values of d/ζ for the experiments in bulk and close to the surface are marked by a square and a circle, respectively.

From this we see the importance of choosing a drive frequency small enough for the fluid to follow the flow cell in the region where the trap is to be calibrated.

APPENDIX C: POWER SPECTRAL DENSITY FOR FINITE MEASUREMENT TIME

In Sec. III we calculated the PSD for the beads' motion, assuming infinite measurement time as well as continuous sampling. In a real experiment, data are collected for a finite time t_{msr} and with a finite sampling frequency f_{sample}. In what follows we are going to assume continuous sampling in time, since the *aliasing* caused by finite sampling time (i) is irrelevant for the discussion here, (ii) is easily accounted for,[2] and (iii) does not occur at all, if oversampling data acquisition electronics is used. Readers feeling uneasy about the idea of continuous sampling need only remind themselves that it is a mathematical ideal, a limit that is achieved in practice by choosing $f_{\mathrm{Nyq}}=f_{\mathrm{sample}}/2 \gg f_{\mathrm{c}}$ and, if aliasing occurs, by leaving frequencies with significant aliasing out of the analysis. Equations (H5) and (H6) in Ref. 2 indicate which frequencies have significant aliasing for a given desired accuracy.

For the finite-time continuous-time Fourier transform of Eq. (5) we now have

$$\tilde{x}_k = \int_{-t_{\mathrm{msr}}/2}^{t_{\mathrm{msr}}/2} \mathrm{d}t\ e^{i2\pi f_k t} x(t), \tag{C1}$$

and the expectation value for the one-sided ($f_k \geqslant 0$) PSD becomes

$$P_k(t_{\mathrm{msr}}) = \frac{2\langle|\tilde{x}_k|^2\rangle}{t_{\mathrm{msr}}} = \frac{D + (f_{\mathrm{drive}} r_k A)^2 t_{\mathrm{msr}}}{\pi^2(f_k^2 + f_{\mathrm{c}}^2)}, \tag{C2}$$

where

$$r_k = \frac{1}{\sqrt{2}} \frac{\sin(\pi(f_k - f_{\mathrm{drive}})t_{\mathrm{msr}})}{(f_k - f_{\mathrm{drive}})t_{\mathrm{msr}}} \tag{C3}$$

gives the shape of the spike in the PSD, referred to as *leakage*;[16] see Fig. 5 of Ref. 27 for peak shapes. Here, $f_k = k/t_{\mathrm{msr}}$, where k is an integer. We have ignored cross terms of the type $\sin(\pi(f_k - f_{\mathrm{drive}})t_{\mathrm{msr}})\sin(\pi(f_k + f_{\mathrm{drive}})t_{\mathrm{msr}})$ in Eq. (C3), as they are typically several orders of magnitude smaller than the terms retained.

The recording time t_{msr} is easily chosen to be an integer multiple of the period of the stage's motion f_{drive}. It can be done even after recording was finished, simply by discarding an incomplete stage period from the recording. A simplification is thereby achieved, $f_{\mathrm{drive}}=f_k$ for some integer k, so the spike consists of a single datum,

$$r_k = \frac{\pi}{\sqrt{2}} \delta_{f_k, f_{\mathrm{drive}}}, \tag{C4}$$

and the PSD becomes

$$P_k(t_{\mathrm{msr}}) = \frac{D}{\pi^2(f_k^2 + f_{\mathrm{c}}^2)} + \frac{f_{\mathrm{drive}}^2 A^2}{2(f_k^2 + f_{\mathrm{c}}^2)} t_{\mathrm{msr}} \delta_{f_k, f_{\mathrm{drive}}}, \tag{C5}$$

where $\delta_{f_k, f_{\mathrm{drive}}}$ is Kronecker's delta. This is the discrete version of the expression given in Eq. (9). We also see that the height of the spike depends linearly on the measurement time t_{msr}. When the measurement time is increased the spike approaches Dirac's delta function,

$$t_{\mathrm{msr}} \delta_{f_k, f_{\mathrm{drive}}} \to \delta(f - f_{\mathrm{drive}}), \quad t_{\mathrm{msr}} \to \infty, \tag{C6}$$

and the expression in Eq. (9) is regained.

APPENDIX D: HYDRODYNAMICALLY CORRECT POWER SPECTRUM ANALYSIS

No general statement can be made regarding which accuracy to expect from a Lorentzian fit. The importance of omitted effects depends on several circumstances.[2,3] As a rule of thumb, we recommend the use of the hydrodynamically correct theory for Brownian motion, if less than 10% systematic error is desired. User-friendly software exists that calibrates with the full theory,[17,18] and one is left with fewer concerns regarding reliability of results.

1. Hydrodynamically correct power spectrum

The hydrodynamically correct power spectrum of Brownian motion of a microsphere that is trapped by a Hookean force is

$$P^{\mathrm{hydro}}(f, R/\ell) = P_T^{\mathrm{hydro}} + P_{\mathrm{response}}^{\mathrm{hydro}}, \tag{D1}$$

where

$$P_T^{\mathrm{hydro}}(f, R/\ell) = \frac{D_0 \mathrm{Re}\{\gamma/\gamma_0\}}{\pi^2((f_{\mathrm{c},0} + f\,\mathrm{Im}\{\gamma/\gamma_0\} - f^2/f_{m,0})^2 + (f\,\mathrm{Re}\{\gamma/\gamma_0\})^2)} \tag{D2}$$

and

$$P_{\mathrm{response}}^{\mathrm{hydro}}(f, R/\ell) = \frac{(A f_{\mathrm{drive}} |\gamma/\gamma_0|)^2 \delta(f - f_{\mathrm{drive}})}{2((f_{\mathrm{c},0} + f\,\mathrm{Im}\{\gamma/\gamma_0\} - f^2/f_{m,0})^2 + (f\,\mathrm{Re}\{\gamma/\gamma_0\})^2)}. \tag{D3}$$

Equation (D2) is the same expression as given in Eq. (34) of Ref. 2 (note, however, Ref. 30). Here $\gamma(f, R/\ell)$ is the frequency-specific drag coefficient that results from solving Stokes equations for the microsphere undergoing linear harmonic motion with frequency f. We assume that this motion takes place parallel to an infinite planar surface that is located a distance ℓ from the center of the microsphere with radius R and give an approximate expression for $\gamma(f, R/\ell)$ below. Using the notation $\gamma_0 = \gamma(0,0) = 6\pi\rho\nu R$, where ρ is the density of the surrounding liquid and ν its kinematic

viscosity, the parameters in Eqs. (D2) and (D3) are $D_0 = k_B T/\gamma_0$, $f_{c,0} = \kappa/(2\pi\gamma_0)$, and $f_{m,0} = \gamma_0/(2\pi m)$, with m the mass of the microsphere. All three parameters are independent of ℓ. They describe bulk values, while all ℓ dependence of the PSD is found in $\gamma(f, R/\ell)/\gamma_0$. In this manner, consistency of experimental power spectra that are recorded with the same bead and trap at different distances to a surface is very easy to check: The values returned for D_0 and $f_{m,0}$ should all be the same, while variation in $f_{c,0}$ arises from variation due to optical aberrations [that depend on ℓ (Ref. 12)].

2. The drag coefficient

The drag coefficient $\gamma(f, R/\ell)$ is not known exactly for $R/\ell > 0$. Deep in bulk, $R/\ell = 0$, and one has Stokes' exact result,[31]

$$\gamma(f,0) = \gamma_{\text{Stokes}}(f) \equiv \gamma_0\left(1 + (1-i)\sqrt{\frac{f}{f_\nu}} - i\frac{2}{9}\frac{f}{f_\nu}\right), \quad \text{(D4)}$$

where $f_\nu = \nu/(\pi R^2)$. At zero frequency one has Faxén's approximate result,[15,32]

$$\gamma(0, R/\ell) = \gamma_{\text{Faxén}}(R/\ell) \equiv \frac{\gamma_0}{1 - 9R/16\ell + R^3/8\ell^3 - 45R^4/256\ell^4 - R^5/16\ell^5 + \cdots}. \quad \text{(D5)}$$

An exact result exists[33] and has been shown numerically[34] to agree with Eq. (D5) to within 1% for $\ell/R \gtrsim 1.4$.

An approximate expression for $\gamma(f, R/\ell)$ is given in Eq. (33) of Ref. 2. At zero frequency, it reproduces Faxén's result up to and including its first order term in R/ℓ. In the spirit of Padé approximants, we rearranged the terms of Eq. (33) of Ref. 2 to

$$\gamma(f, R/\ell) = \frac{\gamma_{\text{Stokes}}(f)}{1 - (9/16)(R/\ell)\{1 - [(1-i)/3]\sqrt{f/f_\nu} + 2if/9f_\nu - (4/3)(1 - e^{-(1-i)(2\ell - R)/\delta})\} + \cdots} \quad \text{(D6)}$$

where $\delta = R\sqrt{f_\nu/f}$ and the series in R/ℓ in the denominator is not known beyond the explicitly shown terms. For $f = 0$ this expression reproduces Faxén's result up to and including its *second* order term in R/ℓ: For $\ell/R > 1.5$ it deviates by less than 0.5% from Faxén's result, and for $\ell/R > 5$ the deviation is smaller than 0.1%. This is a significantly better approximation to Faxén's result, so it must also be a significant improvement at low frequencies, and possibly at all frequencies.

We found that Eq. (D2) agrees with our experimental PSDs down to significantly shorter distances from the surface when $\gamma(f, R/\ell)$ in Eq. (D6) is used instead of Eq. (33) in Ref. 2 (see Refs. 35 and 36).

3. How to fit the ℓ-dependent power spectrum

In order to fit the theoretical power spectrum in Eqs. (D1)–(D3) to the experimental one, the distance ℓ to the surface must be known. We do know the *differences* between the various distances at which we recorded power spectra. It is only the location of the coverslip surface that is unknown.

This location can be determined in several ways: from the fluorescence induced by an evanescent wave, from the effect of the hydrodynamic interaction of the trapped bead with the surface, or by analyzing interference or diffractive patterns (see Ref. 1 and references therein and Refs. 21 and 37). Yet another method relies on pulling on DNA constructs along the axial direction.[38] Most of these methods require a modification of the experimental setup. We used the hydrodynamic interaction of the bead with the surface, similar to that described in Ref. 39 but taking advantage of an improved understanding of the focal shift, as detailed in Ref. 12. This method requires no extra instrumentation.

In principle, one might fit Eqs. (D1)–(D3) simultaneously to all power spectra recorded with a given bead in the trap and let the location of the surface be a fitting parameter. We used a simpler procedure, based on the observation that the distance to the surface is needed only with moderate precision in order to determine the fitting parameters D_0 and $f_{c,0}$ with high precision. This is because the distance occurs only in Eq. (D6) in terms that play a subdominant role in Eqs. (D1)–(D3).

We fitted Eq. (D2) to the thermal background and compared the results from inserting either $\gamma = \gamma_{\text{Faxén}}$ [turning Eq. (D2) into a Lorentzian] or $\gamma = \gamma_{\text{Faxén}}\gamma_{\text{Stokes}}/\gamma_0$. The distance-dependent results for f_c and D were found to agree within 1% for the two approaches. This agreement is partly artificial: We described the parasitic filtering in our diode with Eq. (35) of Ref. 2, fitting its two parameters. This characteristic function absorbed most of the difference between γ_0 and $\gamma_{\text{Stokes}}(f)$.

Einstein's relation then gives a distance-dependent $\gamma_{\text{ex}} = k_B T/D$, while Faxén's law should give the distance dependence $\gamma_{\text{ex}} \approx \gamma_{\text{Faxén}}(R/\ell)$. We therefore fitted Faxén's law to our ℓ-dependent values for γ_{ex}, using the location of the surface as a fitting parameter. The good fits confirmed the procedure.[12]

With ℓ thus known, we know $\gamma(f, R/\ell)$ in Eq. (D6) and can fit the experimental PSDs with the more correct theoretical PSD that results from using Eq. (D6) in Eq. (D2) and D_0 and $f_{c,0}$ as fitting parameters with their *original* interpretation: $D_0 = k_B T/\gamma_0$ and $f_{c,0} = \kappa/(2\pi\gamma_0)$.

Note that although f_ν depends on the radius of the bead and on the kinematic viscosity of the surrounding fluid, it is systematically correct to insert the manufacturer's value for the radius and the room temperature value for the viscosity in f_ν. This is because in Eq. (D6) these small errors occur in a term that is already a small correction.

4. Hydrodynamically correct calibration factor

The hydrodynamically correct theory described above gives

$$W_{\mathrm{th,hydro}} = \int P_{\mathrm{response}}^{\mathrm{hydro}} \mathrm{d}f = \frac{A^2 |\gamma/\gamma_0|^2}{2((f_{\mathrm{c},0}/f_{\mathrm{drive}} + \mathrm{Im}\{\gamma/\gamma_0\} - f_{\mathrm{drive}}/f_{m,0})^2 + (\mathrm{Re}\{\gamma/\gamma_0\})^2)}. \quad \text{(D7)}$$

This expression does not change the calibration factor β by much, compared to what Eq. (13) would give. This is because Einstein's approximate theory for Brownian motion that leads to Eq. (13) is a low-frequency approximation, and f_{drive} is a low frequency compared to the characteristic frequency f_ν of the frequency dependent drag. At room temperature $(f_{\mathrm{drive}}/f_\nu)^{1/2} = 7.2 \times 10^{-3}$ for the 1.54 μm diameter beads we drove at $f_{\mathrm{drive}} = 28$ Hz, and $(f_{\mathrm{drive}}/f_\nu)^{1/2} = 2.6 \times 10^{-3}$ for the 528 nm diameter beads we drove at $f_{\mathrm{drive}} = 32$ Hz. Inertial effects are two orders of magnitude smaller.[2] Comparing with Eq. (13), we see that, in bulk, the hydrodynamically correct theory in our case introduces corrections of 1.5% and 0.5%, respectively, in the interpretation of the power in the spike. In contrast, near a surface the corrections to Eq. (13) are of the opposite sign and a smaller magnitude than the corrections in bulk: for $\ell/R = 10$, $f_{\mathrm{drive}} = 32$ Hz, $f_{\mathrm{c},0} = 2000$ Hz, and $2R = 528$ nm the correction is -0.25%.

[1] K. C. Neuman and S. M. Block, Rev. Sci. Instrum. **75**, 2787 (2004).
[2] K. Berg-Sørensen and H. Flyvbjerg, Rev. Sci. Instrum. **75**, 594 (2004).
[3] K. Berg-Sørensen, E. J. G. Peterman, T. Weber, C. F. Schmidt, and H. Flyvbjerg, Rev. Sci. Instrum. **77**, 063106 (2006).
[4] G. J. Brouhard, H. T. Schek III, and A. J. Hunt, IEEE Trans. Biomed. Eng. **50**, 121 (2003).
[5] S. C. Kuo and M. P. Sheetz, Science **260**, 232 (1993).
[6] R. Simmons, J. Finer, S. Chu, and J. Spudich, Biophys. J. **70**, 1813 (1996).
[7] A common approach calibrates far enough above the coverslip surface to ensure that uncertainty about the height does not affect the calibration significantly. This calibration is then used closer to the surface. If an oil-immersion objective is used, this is an error-prone approach: due to the difference in refractive index between oil and water, the trap stiffness decreases rapidly with distance from the surface—10 μm from the surface—and the stiffness is typically reduced by more than a factor of 2 for beads with a diameter of ~500 nm (Refs. 12, 20, 21, and 42). Thus, one detrimental effect is swapped for another, and calibration errors can be large.
[8] S. B. Smith, Y. Cui, and C. Bustamante, Science **271**, 795 (1996).
[9] M. J. Lang, C. L. Asbury, J. W. Shaevitz, and S. M. Block, Biophys. J. **83**, 491 (2002).
[10] K. C. Vermeulen, J. van Mameren, G. J. M. Stienen, E. J. G.Peterman, G. J. L. Wuite, and C. F. Schmidt, Rev. Sci. Instrum. **77**, 013704 (2006).
[11] M. Capitanio, R. Cicchi, and F. S. Pavone, Eur. Phys. J. B **46**, 1 (2005).
[12] E. Schäffer, S. F. Nørrelykke, and J. Howard (unpublished).
[13] U. Bockelmann, Ph. Thomen, B. Essevaz-Roulet, V. Viasnoff, and F. Heslot, Biophys. J. **82**, 1537 (2002).
[14] See Appendix C for how to square Dirac's delta-function in Eq. (8).
[15] J. Happel and H. Brenner, *Low Reynolds Number Hydrodynamics* (Noordhoff, Leyden, 1973).
[16] F. J. Harris, Proc. IEEE **66**, 51 (1978).
[17] I. M. Tolić-Nørrelykke, K. Berg-Sørensen, and H. Flyvbjerg, Comput. Phys. Commun. **159**, 225 (2004).
[18] P. M. Hansen, I. M. Tolić-Nørrelykke, H. Flyvbjerg, and K. Berg-Sørensen, Comput. Phys. Commun. **174**, 518 (2006).
[19] S. Hell, G. Reiner, C. Cremer, and E. H. K. Stelzer, J. Microsc. **169**, 391 (1993).
[20] E.-L. Florin, A. Pralle, E. H. K. Stelzer, and J. K. H. Hörber, Appl. Phys. A: Mater. Sci. Process. **66**, 75 (1998).
[21] K. C. Neuman, E. A. Abbondanzieri, and S. M. Block, Opt. Lett. **30**, 1318 (2005).
[22] E. J. G. Peterman, F. Gittes, and C. F. Schmidt, Biophys. J. **84**, 1308 (2003).
[23] W. Denk and W. W. Webb, Appl. Opt. **29**, 2382 (1990).
[24] K. Svoboda, C. F. Schmidt, B. J. Schnapp, and S. M. Block, Nature (London) **365**, 721 (1993).
[25] A. Pralle, M. Prummer, E. L. Florin, E. H. K. Stelzer, and J. K. H. Horber, Microsc. Res. Tech. **44**, 378 (1999).
[26] J. Howard and A. J. Hudspeth, Neuron **1**, 189 (1988).
[27] K. Berg-Sørensen, L. Oddershede, E.-L. Florin, and H. Flyvbjerg, J. Appl. Phys. **93**, 3167 (2003).
[28] A. Rohrbach, Phys. Rev. Lett. **95**, 168102 (2005).
[29] L. D. Landau and E. M. Lifshitz, *Fluid Mechanics*, Course of Theoretical Physics Vol. 6 (Pergamon, Oxford, 1959).
[30] Equation (34) in Ref. 2 contains a typographical error: The parameter f_m in this equation is $f_{m,0} = \gamma_0/(2\pi m)$, i.e., not the same as the parameter f_m, which occurs in Eq. (32) in Ref. 2. Systematic naming is achieved, if the latter is referred to as $f_{m^*,0} = \gamma_0/(2\pi m^*)$, i.e., only its name is changed, not its definition in terms of $m^* = m + 2\pi\rho R^3/3$, where ρ is the mass density of the liquid (Ref. 40). This error is *not* repeated in the programs described in Refs. 17 and 18.
[31] G. G. Stokes, Trans. Cambridge Philos. Soc. **9**, 8 (1851).
[32] H. Faxén, Ph.D. thesis, Uppsala, 1921.
[33] M. O'Neill, Mathematika **11**, 67 (1964).
[34] A. J. Goldman, R. G. Cox, and H. Brenner, Chem. Eng. Sci. **22**, 637 (1967).
[35] Consequently, Eq. (D6)'s expression for $\gamma(f, R/\ell)$ has been introduced in the programs described in Refs. 17 and 18 in the latest versions found in *Computer Physics Communication*'s program library (Ref. 41).
[36] Note, however, that a function can approximate another function well, even when their derivatives do *not* approximate each other well. This is the case here: If one considers how Faxén's result $\gamma(0, R/\ell)$ is *approached* by $\gamma(f, R/\ell)$ by expanding Eq. (D6) in powers of $\sqrt{f/f_\nu}$, the approach is incorrect to first order.
[37] P. M. Hansen, J. K. Dreyer, J. Ferkinghoff-Borg, and L. Oddershede, J. Colloid Interface Sci. **287**, 561 (2005).
[38] C. Deufel and M. D. Wang, Biophys. J. **90**, 657 (2006).
[39] M. D. Wang, H. Yin, R. Landick, J. Gelles, and S. M. Block, Biophys. J. **72**, 1335 (1997).
[40] K. Berg-Sørensen and H. Flyvbjerg, Rev. Sci. Instrum. (to be published).
[41] K. Berg-Sørensen and H. Flyvbjerg (private communication).
[42] K. C. Vermeulen, G. J. L. Wuite, G. J. M. Stienen, and C. F. Schmidt, Appl. Opt. **45**, 1812 (2006).
[43] H. Flyvbjerg, Winter Workshop on Biophysics, Aspen, CO, 2–8 January 2005 (unpublished).